A zombie *LIF* gene in elephants is up-regulated by TP53 to induce apoptosis in response to DNA damage

Juan Manuel Vazquez[1], Michael Sulak[1], Sravanthi Chigurupati[1], and Vincent J. Lynch[1,2]

1) Department of Human Genetics, The University of Chicago, Chicago, IL, 60637
2) Department of Organismal Biology and Anatomy, The University of Chicago, Chicago, IL, 60637

* To whom correspondence should be addressed: vjlynch@uchicago.edu

Abstract

Among the evolutionary and developmental constraints on the evolution of very large body sizes is an increased risk of developing cancer because large bodied organisms have more cells that can potentially turn cancerous than small-bodied organisms with fewer cells. This expectation predicts a positive correlation between body size and cancer risk, however, there is no correlation between body size and cancer risk across species; this lack of correlation is often referred to as 'Peto's Paradox'. Here we show that elephants and their extinct relatives (Proboscideans) resolved Peto's Paradox at least in part through re-functionalizing a *leukemia inhibitory factor* pseudogene (*LIF6*) with pro-apoptotic functions. The re-functionalized *LIF* gene is transcriptionally up-regulated by TP53 in response to DNA damage, and translocates to the mitochondria where it induces apoptosis. Phylogenetic analyses of living and extinct Proboscidean *LIF6* genes indicates its TP53 response element evolved coincident with the evolution of large body sizes in the Proboscidean stem-lineage. These results suggest that re-functionalizing of a pro-apoptotic LIF pseudogene may have played a role in the evolution of large body sizes in Proboscideans.

Introduction

The risk of developing cancer places severe constraints on the evolution of large body sizes and long lifespans in animals. If all cells have a similar risk of malignant transformation and equivalent cancer suppression mechanisms, organism with many cells should have a higher risk of developing cancer than organisms with fewer cells. Similarly organisms with long lifespans have more time to accumulate cancer-causing mutations than organisms with shorter lifespans and therefore should also be at an increased risk of developing cancer, a risk that is compounded in large-bodied, long-lived organisms (Cairns, 1975; Caulin and Maley, 2011; Doll, 1971; Peto, 2015; Peto, 1975). Consistent with these expectations, there are strong positive correlations between body size and lifespan and cancer incidence *within* species. In stark contrast, however, there are no correlations between body size or lifespan and cancer risk *between* species; this lack of correlation is often referred to as 'Peto's Paradox' (Caulin and Maley, 2011; Leroi et al., 2003; Peto, 1975). While the ultimate resolution to Peto's paradox is obvious, large bodied and/or long-lived species evolved enhanced cancer protection mechanisms, identifying and characterizing those mechanisms has been challenging.

Among the mechanisms large and long lived animals may have evolved that resolve Peto's paradox are a reduced number of oncogenes and/or an increased number of tumor suppressor genes, among many others (Caulin and Maley, 2011; Leroi et al., 2003; Nunney, 1999). The multifunctional interleukin-6 class cytokine *leukemia inhibitory factor* (*LIF*), for example, can function as either a tumor suppressor or an oncogene depending on the context. Classically LIF functions as an extracellular cytokine by binding the LIF receptor (LIFR) complex, which activates downstream PI3K/AKT, JAK/STAT3, and TGFβ signaling pathways. The *LIF* gene generates at least three transcripts, LIF-D, LIF-M, and LIF-T, which contain alternative first exons spliced to common second and third exons (Haines et al., 1999; Hisaka et al., 2004; Rathjen et al., 1990; Voyle et al., 1999). Remarkably while the LIF-D and LIF-M isoforms are secreted proteins that interact with the LIF receptor (Rathjen et al., 1990; Voyle et al., 1999), the LIF-T isoform lacks a propeptide sequence and is an exclusively intracellular protein (Haines et al., 1999; Voyle et al., 1999) that induces caspase-dependent apoptosis through an unknown mechanism (Haines et al., 2000).

Here we show that the genomes of Paenungulates (elephant, hyrax, and manatee) contain numerous duplicate *LIF* genes, which encode proteins that are structurally similar to LIF-T. While most of these duplicates likely encode non-functional pseudogenes, at least one (*LIF6*) is expressed in elephants and is up-regulated by TP53 in response to DNA damage. LIF6 induces apoptosis when heterologously expressed in cell lines, and is required for the elephant-specific enhanced cell death in response to DNA-damage. Molecular evolutionary analyses of the duplicate *LIF* paralogs indicates that the elephant *LIF6* locus re-evolved into an expressed, functional gene from a pseudogene ancestor after evolving a TP53 response element approximately 31 million years ago. These results suggest that the origin of large body sizes, long lifespans, and enhanced cancer resistance in the elephant lineage evolved coincident with the origin of a zombie *LIF* gene (a reanimated pseudogene that kills cells when expressed) encoding a lethal separation of function mutant.

Results

Repeated segmental duplications increased *LIF* copy number in Paenungulates

We characterized *LIF* copy number in 53 mammalian genomes, including large, long-lived mammals such as the African elephant (*Loxodonta africana*), Bowhead (*Balaena*

mysticetus) and Minke (*Balaenoptera acutorostrata scammoni*) whales, as well as small, long-lived mammals such bats and the naked mole rat. We found that most Mammalian genomes encoded a single *LIF* gene, however, the manatee (*Trichechus manatus*), rock hyrax (*Procavia capensis*), and African elephant genomes contained 6-11 additional copies of *LIF* (**Figure 1**). None of the duplicate *LIF* genes includes the 5'-UTR, coding exon 1, or a paired low complexity (CGAG)n/CT-rich repeat common to the canonical *LIF* genes in elephant, hyrax, manatee, tenrec, and armadillo (**Figure 2A**). Most of the duplicates include complex transposable element insertions within introns one and two, composed of tandem tRNA-Asn-AAC/AFROSINE and AFROSINE3/tRNA-RTE/MIRc elements (**Figure 2A**). Fine mapping of the duplicate ends by reciprocal best BLAT indicates that there is no region of homology upstream of the tRNA-Asn-AAC/AFROSINE elements for duplicates that include exon 2, whereas duplicate *LIF* genes that lack exon 2 have ~150-300bp regions of homology just upstream of the paired AFROSINE3/tRNA-RTE/MIRc elements in intron 2. The *LIF* encoding loci in the hyrax and manatee genomes have not been assembled into large-scale scaffolds, but the African elephant *LIF* loci are located within a 3.5Mb block of chromosome 25 (loxAfr4).

LIF duplicates may result from independent duplication events in the elephant, hyrax, and manatee lineages, ancestral duplications that occurred in the Paenungulate stem-lineage followed by lineage-specific duplication and loss events, or some combination of these processes. We used Bayesian phylogenetic methods to reconstruct the *LIF* gene tree and gene tree reconciliation to reconstruct the pattern of *LIF* duplication and loss events in Paenungulates. Consistent with a combination of ancestral and lineage-specific duplications, our phylogenetic analyses of Paenungulate *LIF* genes identified well-supported clades containing loci from multiple species as well as clades containing loci from only a single species (**Figure 2B**). The reconciled tree identified 17 duplication and 14 loss events (**Figure 2C**). These data indicate that the additional *LIF* genes result from repeated rounds of segmental duplication, perhaps mediated by recombination between repeat elements.

Duplicate *LIF* genes are structurally similar to the LIF-T

Barring transcription initiation from cryptic upstream sites encoding in frame start codons, all duplicate *LIF* genes encode N-terminally truncated variants that are missing exon 1, lack the propeptide sequence, and are similar in primary structures to LIF-T (**Figure 3A**). While some duplicates lack the N-terminal LIFR interaction site (**Figure 3A**), all include the

leucine/isoleucine repeat required for inducing apoptosis (**Figure 3A**) (Haines et al., 2000). Crucial residues that mediate the interaction between LIF and LIFR (**Figure 3B**) (Hudson et al., 1996; Huyton et al., 2007) are relatively well conserved in duplicate LIF proteins, as are specific leucine/isoleucine residues that are required for the pro-apoptotic functions of LIF-T (**Figure 3C**)(Haines et al., 2000). Haines et al. (2000) suggested that the leucine/isoleucine residues of LIF-T are located on a single face of helix B, and may form an amphipathic α-helix. Similar to LIF-T, leucine/isoleucine residues of duplicate LIF proteins are located on a single face of helix B (**Figure 3D**). These data suggest that at least some of the structural features that mediate LIF functions, in particular the pro-apoptotic function(s) of LIF-T, are conserved in duplicate LIFs.

Elephant *LIF6* is up-regulated by p53 in response to DNA damage

If expansion of the *LIF* gene repertoire plays a role in the evolution of enhanced cancer resistance, then one or more of the *LIF* genes should be transcribed. To determine if duplicate *LIF* genes were transcribed, we assembled and quantified elephant *LIF* transcripts with HISAT2 (Kim et al., 2015) and StringTie (Pertea et al., 2015) using deep 100bp paired-end RNA-Seq data (>138 million reads) we previously generated from Asian elephant dermal fibroblasts (Sulak et al., 2016), as well as more shallow (~30 million reads) singe-end sequencing from African elephant dermal fibroblasts (Cortez et al., 2014) and placenta (Sulak et al., 2016), and Asian elephant peripheral blood mononuclear cells (PBMCs) (Reddy et al., 2015). We identified transcripts corresponding to the LIF-D, LIF-M, and LIF-T isoforms of the canonical *LIF1* gene, and one transcript of a duplicate *LIF* gene (*LIF6*) in Asian elephant dermal fibroblasts (**Figure 4A**); *LIF6* expression was extremely low (0.33 transcripts per million), as might be expected for a pro-apoptotic gene. No other RNA-Seq dataset identified duplicate LIF transcripts.

Previous studies have shown that TP53 regulates basal and inducible transcription of *LIF* in response to DNA damage through a binding site located in *LIF* intron 1 (Baxter and Milner, 2010; Hu et al., 2007), suggesting that duplicate *LIF* genes may be regulated by TP53. Therefore we computationally predicted TP53 biding sites within a 3kb window around Atlantogenatan *LIF* genes and identified putative binding sites in the first intron of African elephant, hyrax, manatee, tenrec, and armadillo *LIF1* genes whereas the only duplicate *LIF* gene with a putative pTP53 binding site was elephant *LIF6* (**Figure 3B**). Next we treated elephant and hyrax primary dermal fibroblasts (manatee cell lines are unavailable) with the DNA

damaging agent doxorubicin (DOX) or the MDM2 antagonist nutlin-3a and quantified the transcription of canonical and duplicate *LIF* genes by qRT-PCR. DOX treatment induced *LIF6* expression 8.18-fold (Wilcox test, $P=1.54\times10^{-6}$) and nutlin-3a induced *LIF6* expression 16.06-fold (Wilcox test, $P=1.00\times10^{-4}$), which was almost completely attenuated by siRNA mediated TP53 knockdown in African elephant fibroblasts (**Figure 4B**). In contrast we observed no expression of the other duplicate *LIF* genes in African elephant fibroblasts or any *LIF* duplicate in hyrax fibroblasts. These data suggest that while *LIF6* encodes an expressed gene in elephants, the other *LIF* duplicates are either induced by different signals or are pseudogenes.

To test if the putative TP53 binding site upstream of elephant *LIF6* was a functional TP53 response element, we cloned the –1100bp to +30bp region of the African elephant *LIF6* gene into the pGL3-Basic[minP] luciferase reporter vector and tested its regulatory ability in dual luciferase reporter assays. We found the African elephant *LIF6* upstream region had no affect on basal luciferase expression (Wilcox test, $P=0.53$) in transiently transfected African elephant fibroblasts. In contrast, both DOX (Wilcox test, $P=1.37\times10^{-8}$) and nutlin-3a (Wilcox test, $P=1.37\times10^{-8}$) strongly increased luciferase expression (**Figure 4C**), which was almost completely abrogated (Wilcox test, $P=1.37\times10^{-8}$) by deletion of the putative TP53 binding-site (**Figure 4C**). Thus, we conclude that elephant *LIF6* is up-regulated by TP53 in response to DNA damage.

Elephant LIF6 contributes to the augmented DNA-damage response in elephants

We have previously shown that elephant cells evolved to be extremely sensitive to genotoxic stress and induce apoptosis at lower levels of DNA damage than their closest living relatives (Sulak et al., 2016). To test the contribution of *LIF6* to this derived sensitivity, we treated African elephant dermal fibroblasts with DOX or nutlin-3a and either an siRNA specifically targeting *LIF6* or a control siRNA and assayed cell viability, cytotoxicity, and apoptosis using an ApoTox-Glo assay 24 hours after treatment. Both DOX (Wilcox test, $P=3.33\times10^{-9}$) and nutlin-3a (Wilcox test, $P=3.33\times10^{-9}$) reduced cell viability ~85%, which was attenuated 5-15% by *LIF6* knockdown in DOX (Wilcox test, $P=1.33\times10^{-8}$) or nutlin-3a (Wilcox test, $P=3.33\times10^{-9}$) treated cells (**Figure 5**). While neither DOX not nutlin-3a induced cytotoxicity (**Figure 5**), both DOX (4.05-fold, Wilcox test, $P=3.33\times10^{-9}$) and nutlin-3a (2.64-fold, Wilcox test, $P=3.33\times10^{-9}$) induced apoptosis (**Figure 5**). Thus, LIF6 contributes to the augmented apoptotic response that evolved in the elephant lineage.

Elephant LIF6 induces mitochondrial dysfunction and caspase-dependent apoptosis

To infer the mechanism(s) by which LIF6 contributes to the induction of apoptosis, we first determined the sub-cellular localization of a LIF6–eGFP fusion protein. Unlike LIF-T, which has diffuse cytoplasmic and nuclear localization (Haines et al., 2000), we found that LIF6–eGFP was localized in discrete foci that co-localized with MitoTracker Red CM-H2XRos stained mitochondria (**Figure 6A).** Mitochondria are critical regulators of cell death, with distinct pathways and molecular effectors underlying death through either apoptosis (Karch et al., 2013; Tait and Green, 2010) or necrosis (Tait and Green, 2010; Vaseva et al., 2012). During apoptosis, for example, the Bcl-2 family members Bax/Bak form large pores in the outer mitochondrial membrane that allow cytochrome c to be released into the cytosol thereby activating the caspase cascade (Karch et al., 2013; Tait and Green, 2010). In contrast, during necrosis, Bax/Bak in the outer membrane interact with the cyclophilin D (CypD) and the inner membrane complex leading to the opening of the mitochondrial permeability transition pore (MPTP), loss of mitochondrial membrane potential (MMP), swelling, and eventual rupture (Tait and Green, 2010; Vaseva et al., 2012).

To test if LIF6 over-expression is sufficient to induce apoptosis, we transiently transfected Chinese hamster ovary (CHO) cells (which do not express LIFR) with an expression vector encoding the African elephant *LIF6* gene and assayed the induction of apoptosis with an ApoTox-Glo triplex assay. Overexpression of LIF6 induced apoptosis 5.38-fold (Wilcox test, $P=3.33\times10^{-9}$) 24 hours after transfection, consistent with a pro-apoptotic function (**Figure 6B**). Induction of apoptosis by LIF6, however, was almost completely blocked by co-treatment with the irreversible broad-spectrum caspase inhibitor Z-VAD-FMK (**Figure 6B**). In contrast, cyclosporine A (CsA) treatment, which inhibits CypD and opening of the MPTP, had no effects on LIF6 induced apoptosis (**Figure 6B**). To test if LIF6 induced apoptosis is dependent upon Bax and Bak, we over-expressed LIF6 in Bax/Bak knockout mouse embryonic fibroblasts (MEFs) but did not observe an induction of apoptosis. Thus *LIF6* is sufficient to induce caspase-dependent apoptosis mediated through Bax/Bak and independent of MPTP opening.

Elephant *LIF6* is a refunctionalized pseudogene

We reasoned that because elephant *LIF6* is deeply nested within the duplicate *LIF* clade, is the only expressed duplicate, and is the only duplicate with a TP53 response element, than most duplicate *LIF* genes are (likely) pseudogenes, suggesting elephant *LIF6* re-evolved into a

functional gene from a pseudogene ancestor. To test this hypothesis and reconstruct the evolutionary history of the *LIF6* gene in Proboscidean lineage with greater phylogenetic resolution, we annotated *LIF6* locus in extinct Elephantids including the woolly mammoth (*Mammuthus primigenius*), Columbian mammoth (*Mammuthus columbi*), and straight-tusked elephant (*Palaeoloxodon antiquus*), and the American Mastodon (*Mammut americanum*), an extinct Mammutid. We found that the genomes of each extinct Proboscidean contained a *LIF6* gene with coding potential similar to the African and Asian elephant *LIF6* genes as well as the TP53 binding-site, indicating that *LIF6* evolved to be a TP53 target gene in the stem-lineage of Proboscideans.

We next we used a variant of the branch-sites random effects likelihood method (RELAX) to test if the intensity of selection on duplicate *LIF* genes was relaxed, as expected for pseudogenes. The RELAX method fits a codon model with three d_N/d_S (ω) rate classes to the phylogeny (null model), then tests for relaxed/intensified selection by incorporating a selection intensity parameter (K) to the inferred ω values, relaxed selection (both positive and negative) is inferred when K<1 and selection intensification inferred when K>1. As expected for pseudogenes, *LIF* duplicates (other than Proboscidean *LIF6* genes) had significant evidence for a relaxation in the intensity of selection (Table 1; K=0.36, LRT=42.19, P=8.26×10^{-11}) as did the Proboscidean *LIF6* stem-lineage (K=0.00, LRT=3.84, P=0.05). In contrast, Proboscidean *LIF6* genes had significant evidence for selection intensification (Table 2; K=50, LRT=4.46, P=0.03), consistent with the reacquisition of constraints after refunctionalization.

Finally we inferred a Bayesian time-calibrated phylogeny of Atlantogenatan *LIF* genes, including *LIF6* from African and Asian elephant, woolly and Columbian mammoth, straight-tusked elephant, and American Mastodon, to place upper and lower bounds on when the Proboscidean *LIF6* gene may have refunctionalized (**Figure 7A**). We found that estimated divergence date of the Proboscideans *LIF6* lineage was ~59 MYA (95% HPD: 61-57 MYA) whereas the divergence of Proboscideans was ~26 MYA (95% HPD: 23.28 MYA). These data indicate that the Proboscidean *LIF6* gene refunctionalized during the origin of large body sizes in this lineage, although precisely when within this time interval is unclear (**Figure 7B**).

Discussion

One of the major developmental constraints on the evolution of large body sizes and long lifespans in animals is an increased risk of developing cancer, however, while there is a strong correlation between body size and cancer risk within species no such correlation exists between species. On the one had the resolution of this paradox is trivial, large and long-lived organisms evolved enhanced cancer suppression mechanisms, however, the identification and functional characterization of those mechanisms has thus far been elusive. Among the mechanisms large bodied, long lived animals may have evolved that reduce cancer risk are a decrease in the copy number of oncogenes, an increase in the copy number of tumor suppressor genes (Abegglen et al., 2015; Caulin and Maley, 2011; Leroi et al., 2003; Nunney, 1999; Sulak et al., 2016), increased sensitivity to DNA damage, decreased somatic mutation rates, reduced metabolic rates leading to decreased free radical production, reduced retroviral activity and load (Katzourakis et al., 2014), increased immune surveillance, and selection for "cheater" tumors that parasitize the growth of other tumors (Nagy et al., 2007), among potentially many others.

A comprehensive analyses of genetic changes associated with the resolution of Peto's paradox in the elephant lineage has yet to be performed, but candidate gene studies have identified functional duplicates of the master tumor suppressor p53 as well as putative duplicate of other tumor suppressor genes (Abegglen et al., 2015; Caulin et al., 2015; Sulak et al., 2016). Caulin et al, for example, characterized the copy number of 830 tumor-suppressor genes (Higgins et al., 2007) across 36 mammals and identified 382 putative duplicates including five copies of *LIF* in African elephants, seven in hyrax, and three in tenrec. Here we show that an incomplete duplication of the *LIF* gene in the Paenungulate stem-lineage generated a duplicate missing the proximal promoter and exon 1, generating a gene with similar structure to the LIF-T isoform (Haines et al., 1999). Additional duplications of this original duplicate increased *LIF* copy number in Paenungulates, however, most *LIF* duplicates lack regulatory elements, are not expressed in elephant or hyrax fibroblasts (manatee cells or tissues are unavailable), and are therefore likely pseudogenes (with the exception of elephant *LIF6*).

While random DNA sequences can evolve into promoters with only a few substitutions (Yona et al., 2017), there should be strong selection against the origin of constitutively active

enhancers/promoters for pro-apoptotic pseudogenes because their expression will be toxic, implying refunctionalizing LIF pseudogenes may impose a potential evolutionary cost. One of the few ways to refunctionalize pro-apoptotic pseudogenes is through the gain of inducible regulatory elements that appropriately respond to specific stimuli, such as the origin of the TP53 response element that brought *LIF6* under the transcriptional control of TP53. Although precisely dating the origin of the TP53 binding site that drives *LIF6* expression is not possible, it evolved before the divergence of mastodons and the modern elephant lineage. These data indicate that *LIF6* refunctionalized in the stem-lineage of Proboscideans coincident with the origin of large body sizes, and suggests reanimation of *LIF6* contributed to the evolution of enhancer cancer resistance in Proboscideans.

Although the precise mechanisms by which mitochondrial dysfunction leads to apoptosis are uncertain, during early stages of apoptosis the pro-death Bcl-2 family members Bax and Bak hetero- and homo-oligomerize within the mitochondrial outer membrane leading to permeabilization (MOMP) and the release of pro-apoptotic protein such as cytochrome c (Karch et al., 2013; 2015). In contrast, during necrosis the collapse of the MMP and the opening of the mitochondrial permeability transition pore (MPTP) leads to mitochondrial swelling, rupture, and cell death (Ly et al., 2003). Our observations that cyclosporine A (CsA) did not inhibit LIF6 induced apoptosis, but that LIF6 over-expression was insufficient to induce apoptosis in Bax/Bak null MEFs suggests that LIF6 functions in a manner analogous to the pro-apoptotic Bcl-2 family members by inducing the opening of the outer mitochondrial membrane pore. The molecular mechanisms by which LIF6 induces apoptosis, however, are unclear and the focus of continued studies.

Materials and methods

Identification of *LIF* genes in Mammalian genomes

We used BLAT to search for *LIF* genes in 53 Sarcopterygian genomes using the human LIF protein sequences as an initial query. After identifying the canonical *LIF* gene from each species, we used the nucleotide sequences corresponding to this *LIF* CDS as the query sequence for additional BLAT searches within that species genome. To further confirm the orthology of each *LIF* gene we used a reciprocal best BLAT approach, sequentially using the putative CDS of each *LIF* gene as a query against the human genome; in each case the query gene was identified as *LIF*. Finally we used the putative amino acid sequence of the LIF protein as a query sequence in a BLAT search.

We thus used BLAT to characterize the *LIF* copy number in Human (*Homo sapiens*; GRCh37/hg19), Chimp (*Pan troglodytes*; CSAC 2.1.4/panTro4), Gorilla (*Gorilla gorilla gorilla*; gorGor3.1/gorGor3), Orangutan (*Pongo pygmaeus abelii*; WUGSC 2.0.2/ponAbe2), Gibbon (*Nomascus leucogenys*; GGSC Nleu3.0/nomLeu3), Rhesus (*Macaca mulatta*; BGI CR_1.0/rheMac3), Baboon (*Papio hamadryas*; Baylor Pham_1.0/papHam1), Marmoset (*Callithrix jacchus*; WUGSC 3.2/calJac3), Squirrel monkey (*Saimiri boliviensis*; Broad/saiBol1), Tarsier (*Tarsius syrichta*; Tarsius_syrichta2.0.1/tarSyr2), Bushbaby (*Otolemur garnettii*; Broad/otoGar3), Mouse lemur (*Microcebus murinus*; Broad/micMur1), Chinese tree shrew (*Tupaia chinensis*; TupChi_1.0/tupChi1), Squirrel (*Spermophilus tridecemlineatus*; Broad/speTri2), Mouse (*Mus musculus*; GRCm38/mm10), Rat (*Rattus norvegicus*; RGSC 5.0/rn5), Naked mole-rat (*Heterocephalus glaber*; Broad HetGla_female_1.0/hetGla2), Guinea pig (*Cavia porcellus*; Broad/cavPor3), Rabbit (*Oryctolagus cuniculus*; Broad/oryCun2), Pika (*Ochotona princeps*; OchPri3.0/ochPri3), Kangaroo rat (*Dipodomys ordii*; Broad/dipOrd1), Chinese hamster (*Cricetulus griseus*; C_griseus_v1.0/criGri1), Pig (*Sus scrofa*; SGSC Sscrofa10.2/susScr3), Alpaca (*Vicugna pacos*; Vicugna_pacos-2.0.1/vicPac2), Dolphin (*Tursiops truncatus*; Baylor Ttru_1.4/turTru2), Cow (*Bos taurus*; Baylor Btau_4.6.1/bosTau7), Sheep (*Ovis aries*; ISGC Oar_v3.1/oviAri3), Horse (*Equus caballus*; Broad/equCab2), White rhinoceros (*Ceratotherium simum*; CerSimSim1.0/cerSim1), Cat (*Felis catus*; ICGSC Felis_catus 6.2/felCat5), Dog (*Canis lupus familiaris*; Broad CanFam3.1/canFam3), Ferret *(Mustela putorius furo*; MusPutFur1.0/musFur1), Panda (*Ailuropoda melanoleuca*; BGI-Shenzhen 1.0/ailMel1), Megabat (*Pteropus vampyrus*; Broad/pteVam1), Microbat (*Myotis*

lucifugus; Broad Institute Myoluc2.0/myoLuc2), Hedgehog (*Erinaceus europaeus*; EriEur2.0/eriEur2), Shrew (*Sorex araneus*; Broad/sorAra2), Minke whale (*Balaenoptera acutorostrata scammoni*; balAcu1), Bowhead Whale (*Balaena mysticetus*; v1.0), Rock hyrax (*Procavia capensis*; Broad/proCap1), Sloth (*Choloepus hoffmanni*; Broad/choHof1), Elephant (*Loxodonta africana*; Broad/loxAfr3), Cape elephant shrew (*Elephantulus edwardii*; EleEdw1.0/eleEdw1), Manatee (*Trichechus manatus latirostris*; Broad v1.0/triMan1), Tenrec (*Echinops telfairi*; Broad/echTel2), Aardvark (*Orycteropus afer afer*; OryAfe1.0/oryAfe1), Armadillo (*Dasypus novemcinctus*; Baylor/dasNov3), Opossum (*Monodelphis domestica*; Broad/monDom5), Tasmanian devil (*Sarcophilus harrisii*; WTSI Devil_ref v7.0/sarHar1), Wallaby (*Macropus eugenii*; TWGS Meug_1.1/macEug2), and Platypus (*Ornithorhynchus anatinus*; WUGSC 5.0.1/ornAna1).

Phylogenetic analyses and gene tree reconciliation of Paenungulate *LIF* genes

The phylogeny of *LIF* genes were estimated using an alignment of the *LIF* loci from the African elephant, hyrax, manatee, tenrec, and armadillo genomes and BEAST (v1.8.3) (Rohland et al., 2010). We used the HKY85 substitution, which was chosen as the best model using HyPhy, empirical nucleotide frequencies (+F), a proportion of invariable sites estimated from the data (+I), four gamma distributed rate categories (+G), an uncorrelated random local clock to model substitution rate variation across lineages, a Yule speciation tree prior, uniform priors for the GTR substitution parameters, gamma shape parameter, proportion of invariant sites parameter, and nucleotide frequency parameter. We used an Unweighted Pair Group Arithmetic Mean (UPGMA) starting tree. The analysis was run for 10 million generations and sampled every 1000 generations with a burn-in of 1000 sampled trees; convergence was assessed using Tracer, which indicated convergence was reached rapidly (within 100,000 generations). We used Notung v2.6 (Chen et al., 2000) to reconcile the gene and species trees.

Gene expression data (Analyses of RNA-Seq data and RT-PCR)

To determine if duplicate *LIF* genes were basally transcribed, we assembled and quantified elephant *LIF* transcripts with HISAT2 (Kim et al., 2015) and StringTie (Pertea et al., 2015) using deep 100bp paired-end RNA-Seq data (>138 million reads) we previously generated from Asian elephant dermal fibroblasts (Sulak et al., 2016), as well as more shallow (~30 million reads) singe-end sequencing from African elephant dermal fibroblasts (Cortez et al.,

2014) and placenta (Sulak et al., 2016), and Asian elephant peripheral blood mononuclear cells (PBMCs) (Reddy et al., 2015). HISAT2 and StringTie were run on the Galaxy web-based platform (https://usegalaxy.org) (Afgan et al., 2016) using default settings, and without a guide GTF/GFF file.

We determined if *LIF* transcription was induced by DNA damage and p53 activation in African elephant Primary fibroblasts (San Diego Frozen Zoo) using RT-PCR and primers designed to amplify elephant duplicate *LIF* genes, including LIF1-F: 5'-GCACAGAGAAGGACAAGCTG-3', LIF1-R: 5'-CACGTGGTACTTGTTGCACA-3', LIF6-F: 5'-CAGCTAGACTTCGTGGCAAC-3', LIF6-R: 5'-AGCTCAGTGATGACCTGCTT-3', LIF3-R: 5'-TCTTTGGCTGAGGTGTAGGG-3', LIF4-F: 5'-GGCACGGAAAAGGACAAGTT-3', LIF4-R: 5'-GCCGTGCGTACTTTATCAGG-3', LIF5-F: 5'-CTCCACAGCAAGCTCAAGTC-3', LIF5-R: 5'-GGGGATGAGCTGTGTGTACT-3'. African elephant Primary fibroblasts (San Diego Frozen Zoo) were grown to 80% confluency in T-75 culture flasks at 37℃/5% CO_2 in a culture medium consisting of FGM/EMEM (1:1) supplemented with insulin, FGF, 6% FBS and Gentamicin/Amphotericin B (FGM-2, singlequots, Clonetics/Lonza). At 80% confluency, cells were harvested and seeded into 6-well culture plates at ~10,000 cells/well. Once cells recovered to 80% confluency they were treated with either vehicle control, 50um Doxorubicin, or 50um Nutlin-3a.

Total RNA was extracted using the RNAeasy Plus Mini kit (Qiagen), then DNase treated (Turbo DNA-*free* kit, Ambion) and reverse-transcribed using an olgio-dT primer for cDNA synthesis (Maxima H Minus First Strand cDNA Synthesis kit, Thermo Scientific). Control RT reactions were otherwise processed identically, except for the omission of reverse transcriptase from the reaction mixture. RT products were PCR-amplified for 45 cycles of 94°/20 seconds, 56°/30 seconds, 72°/30 seconds using a BioRad CFX96 Real Time qPCR detection system and SYBR Green master mix (QuantiTect, Qiagen). PCR products were electrophoresed on 3% agarose gels for 1 hour at 100 volts, stained with SYBR safe, and imaged in a digital gel box (ChemiDoc MP, BioRad) to visualize relative amplicon sizes.

Luciferase assay and cell culture

We used the JASPAR database of transcription factor binding site (TFBS) motifs (Mathelier et al., 2015)to computationally predict putative TFBSs within a 3kb window around Atlantogenatan *LIF* genes and identified matches for the TP53 motif (MA0106.3), including a match (sequence: CACATGTCCTGGCAACCT, score: 8.22, relative score: 0.82) ~1kb upstream of the African elephant *LIF6* start codon. To test if the putative p53 binding site upstream of elephant *LIF6* was a functional p53 response element, we synthesized (GeneScript) and cloned the –1100bp to +30bp region of the African elephant *LIF6* gene (loxAfr3_dna range=scaffold_68:4294134-4295330 strand=+ repeatMasking=none) and a mutant lacking the CACATGTCCTGGCAACCT sequence into the pGL3-Basic[minP] luciferase reporter vector.

African elephant Primary fibroblasts (San Diego Frozen Zoo) were grown to 80% confluency in T-75 culture flasks at 37℃/5% CO_2 in a culture medium consisting of FGM/EMEM (1:1) supplemented with insulin, FGF, 6% FBS and Gentamicin/Amphotericin B (FGM-2, singlequots, Clonetics/Lonza). At 80% confluency, cells were harvested and seeded into 96-well white culture plates at ~10,000 cells/well. 24 hours later cells were transfected using Lipofectamine LTX and either 100g of the pGL3-Basic[minP], pGL3-Basic[minP] –1100bp to +30bp, pGL3-Basic[minP] -1100bp–+30bp Δp53TFBS luciferase reporter vectors and 1ng of the pGL4.74[*hRluc*/TK] Renilla control reporter vector according the standard protocol with 0.5 ul/well of Lipofectamine LTX Reagent and 0.1ul/well of PLUS Reagent. 24 hours after transfection cells were treated with either vehicle control, 50um Doxorubicin, or 50um Nutlin-3a. Luciferase expression was assayed 48 hours after drug treatment, using the Dual-Luciferase Reporter Assay System (Promega) in a GloMax-Multi+ Reader (Promega). For all experiments luciferase expression was standardized to Renilla expression to control for differences transfection efficiency across samples; Luc./Renilla data is standardized to (Luc./Renilla) expression in untreated control cells. Each luciferase experiment was replicated three independent times, with 8-16 biological replicates per treatment and control group.

ApoTox-Glo Viability/Cytotoxicity/Apoptosis experiments

African elephant Primary fibroblasts were grown to 80% confluency in T-75 culture flasks at 37℃/5% CO_2 in a culture medium consisting of FGM/EMEM (1:1) supplemented with insulin,

FGF, 6% FBS and Gentamicin/Amphotericin B (FGM-2, singlequots, Clonetics/Lonza). 10^4 cells were seeded into each well of an opaque bottomed 96-well plate, leaving a column with no cells (background control); each 96-well plate contained each species. Cells were treated with 50uM Doxorubicin or 50uM Nutlin-3a with at least four biological replicates for each condition. After 18 hrs of incubation with each drug, cell viability, cytotoxicity, and caspase-3/7 activity were measured using the ApoTox-Glo Triplex Assay (Promega) in a GloMax-Multi+ Reader (Promega). Data were standardized to no-drug control cells. ApoTox-Glo Triplex Assays were replicated three independent times.

siRNAs designed to specifically-target the elephant *LIF6* gene. Sequences of the three LIF-specific siRNAs used are as follows: 1) 5'-GAAUAUACCUGGAGGAAUGUU-3', 2) 5'-GGAAGGAGGCCAUGAUGAAUU-3', 3) 5'-CACAAUAAGACUAGGAUAUUU-3' (Dharmacon). African elephant Primary fibroblasts were transfected with equimolar amounts of each siRNA using Lipofectamine LTX, and assayed for cell viability/toxicity/apoptosis with an ApoTox-Glo assay 48 hours later. We also validated efficiency of the knockdown via qRT-PCR using the primer sets described earlier, which specifically the *LIF6* gene, and confirmed the combination of all three *LIF6* siRNAs was ~88%.

To determine if LIF6 was sufficient to induce apoptosis we synthesized and cloned (GeneScript) the African elephant LIF6 gene into the pcDNA3.1+C-DYK expression vector, which adds at DYK epitope tag immediately C-terminal to the LIF6 protein. We transiently transfected Chinese hamster ovary (CHO) cells with LIF6_ pcDNA3.1+C-DYK expression vector using Lipofectamine LTX according to manufacturer protocol and as described above, and assayed cell viability, cytotoxicity, and the induction of apoptosis using an ApoTox-Glo triplex assay. CHO cells and Bax/Bak (ATCC CRL-2913) MEFs were cultured as described above for African elephant Primary fibroblasts.

Evolutionary analyses of LIF genes

We used a Bayesian approach to date *LIF* duplication events implemented in BEAST (v1.8.3) (Rohland et al., 2010), including all identified African elephant, hyrax, and manatee *LIF* duplicates, as well as cannonical *LIF* genes from armadillo, sloth, aardvark, golden mole, and *LIF6* genes from Asian elephant, woolly and Columbian mammoth, straight-tusked elephant, and American Mastodon (unpublished data, Palkopoulou et al. in preparation). We used the

GTR substitution, which was chosen as the best model using HyPhy, empirical nucleotide frequencies (+F), a proportion of invariable sites estimated from the data (+I), four gamma distributed rate categories (+G) with the shape parameter estimated from the data, an uncorrelated random local clock to model substitution rate variation across lineages, a Yule speciation tree prior, uniform priors for the GTR substitution parameters, gamma shape parameter, proportion of invariant sites parameter, and nucleotide frequency parameter. We used an Unweighted Pair Group Arithmetic Mean (UPGMA) starting tree. The analysis was run for 10 million generations and sampled every 1000 generations with a burn-in of 1000 sampled trees; convergence was assessed using Tracer, which indicated convergence was reached rapidly (within 100,000 generations).

To constrain nodes we used normal priors with estimated confidence intervals, the root node was constrained to be 105 MYA, the root of Xenarthra was constrained to be 66 MYA, the root of Afrosoricida was constrained to be 70 MYA, the root of Afrosoricida-Macroselidea divergence constrained to be 75 MYA, the Elephantidea root was constrained to be 7.5 MYA, the Afrotheria root was constrained to be 83 MYA, the Paeungulata root was constrained to be 68 MYA, and the Proboscidea root was constrained to be 16 MYA. Divergence dates were obtained from www.timetree.org using the 'Expert Result' divergence dates.

We used the RELAX method to (Wertheim et al., 2015) test if duplicate LIF genes experienced a relaxation of the intensity of selection using the DataMonkey web server (Delport et al., 2010). The alignment included all duplicate LIF genes identified in the African elephant, hyrax, and manatee genomes, as well as cannonical *LIF* genes from armadillo, sloth, aardvark, golden mole, and *LIF6* genes from Asian elephant, woolly and Columbian mammoth, straight-tusked elephant, and American Mastodon. Alignment confidence was assessed using GUIDANCE2 (Sela et al., 2015) with the MAFFT (Katoh et al., 2005) algorithm and 100 bootstrap replicates.

Acknowledgements

The authors would like to thank Eleftheria Palkopoulou and David Reich (Harvard Medical School), the Broad Institute, Michael Hofreiter (University of Potsdam) and Hendrik Poinar (McMaster University) for providing access to the Proboscidean sequences, and Ute M. Moll for providing the Bax/Bak KO MEF cell line.

References

Abegglen, L.M., Caulin, A.F., Chan, A., Lee, K., Robinson, R., Campbell, M.S., Kiso, W.K., Schmitt, D.L., Waddell, P.J., Bhaskara, S., et al. (2015). Potential Mechanisms for Cancer Resistance in Elephants and Comparative Cellular Response to DNA Damage in Humans. Jama *314*, 1850–1860.

Afgan, E., Baker, D., van den Beek, M., Blankenberg, D., Bouvier, D., Čech, M., Chilton, J., Clements, D., Coraor, N., Eberhard, C., et al. (2016). The Galaxy platform for accessible, reproducible and collaborative biomedical analyses: 2016 update. Nucleic Acids Res. *44*, W3–W10.

Baxter, E.W., and Milner, J. (2010). p53 Regulates LIF expression in human medulloblastoma cells. J. Neurooncol. *97*, 373–382.

Cairns, J. (1975). Mutation selection and the natural history of cancer. Nature *255*, 197–200.

Caulin, A.F., and Maley, C.C. (2011). Peto“s Paradox: evolution”s prescription for cancer prevention. Trends Ecol. Evol. (Amst.) *26*, 175–182.

Caulin, A.F., Graham, T.A., Wang, L.-S., and Maley, C.C. (2015). Solutions to Peto's paradox revealed by mathematical modelling and cross-species cancer gene analysis. Philos. Trans. R. Soc. Lond., B, Biol. Sci. *370*.

Chen, K., Durand, D., and Farach-Colton, M. (2000). NOTUNG: a program for dating gene duplications and optimizing gene family trees. J. Comput. Biol. *7*, 429–447.

Cortez, D., Marin, R., Toledo-Flores, D., Froidevaux, L., Liechti, A., Waters, P.D., Grutzner, F., and Kaessmann, H. (2014). Origins and functional evolution of Y chromosomes across mammals. Nature *508*, 488–493.

Delport, W., Poon, A.F.Y., Frost, S.D.W., and Kosakovsky Pond, S.L. (2010). Datamonkey 2010: a suite of phylogenetic analysis tools for evolutionary biology. Bioinformatics *26*, 2455–2457.

Doll, R. (1971). The age distribution of cancer: implications for models of carcinogenesis. Journal of the Royal Statistical Society Series a (….

Haines, B.P., Voyle, R.B., and Rathjen, P.D. (2000). Intracellular and extracellular leukemia inhibitory factor proteins have different cellular activities that are mediated by distinct protein motifs. Mol. Biol. Cell *11*, 1369–1383.

Haines, B.P., Voyle, R.B., Pelton, T.A., Forrest, R., and Rathjen, P.D. (1999). Complex conserved organization of the mammalian leukemia inhibitory factor gene: regulated expression of intracellular and extracellular cytokines. J. Immunol. *162*, 4637–4646.

Higgins, M.E., Claremont, M., Major, J.E., Sander, C., and Lash, A.E. (2007). CancerGenes: a gene selection resource for cancer genome projects. Nucleic Acids Res. *35*, D721–D726.

Hisaka, T., Desmoulière, A., Taupin, J.-L., Daburon, S., Neaud, V., Senant, N., Blanc, J.-F.,

Moreau, J.-F., and Rosenbaum, J. (2004). Expression of leukemia inhibitory factor (LIF) and its receptor gp190 in human liver and in cultured human liver myofibroblasts. Cloning of new isoforms of LIF mRNA. Comp Hepatol *3*, 10.

Hu, W., Feng, Z., Teresky, A.K., and Levine, A.J. (2007). p53 regulates maternal reproduction through LIF. Nature *450*, 721–724.

Hudson, K.R., Vernallis, A.B., and Heath, J.K. (1996). Characterization of the receptor binding sites of human leukemia inhibitory factor and creation of antagonists. J. Biol. Chem. *271*, 11971–11978.

Huyton, T., Zhang, J.-G., Luo, C.S., Lou, M.-Z., Hilton, D.J., Nicola, N.A., and Garrett, T.P.J. (2007). An unusual cytokine:Ig-domain interaction revealed in the crystal structure of leukemia inhibitory factor (LIF) in complex with the LIF receptor. Proc. Natl. Acad. Sci. U.S.a. *104*, 12737–12742.

Karch, J., Kanisicak, O., Brody, M.J., Sargent, M.A., Michael, D.M., and Molkentin, J.D. (2015). Necroptosis Interfaces with MOMP and the MPTP in Mediating Cell Death. PLoS ONE *10*, e0130520.

Karch, J., Kwong, J.Q., Burr, A.R., Sargent, M.A., Elrod, J.W., Peixoto, P.M., Martinez-Caballero, S., Osinska, H., Cheng, E.H.-Y., Robbins, J., et al. (2013). Bax and Bak function as the outer membrane component of the mitochondrial permeability pore in regulating necrotic cell death in mice. eLife *2*, e00772.

Katoh, K., Kuma, K.-I., Toh, H., and Miyata, T. (2005). MAFFT version 5: improvement in accuracy of multiple sequence alignment. Nucleic Acids Res. *33*, 511–518.

Katzourakis, A., Magiorkinis, G., Lim, A.G., Gupta, S., Belshaw, R., and Gifford, R. (2014). Larger Mammalian body size leads to lower retroviral activity. PLoS Pathog. *10*, e1004214.

Kim, D., Langmead, B., and Salzberg, S.L. (2015). HISAT: a fast spliced aligner with low memory requirements. Nat. Methods *12*, 357–360.

Leroi, A.M., Koufopanou, V., and Burt, A. (2003). Cancer selection. Nat. Rev. Cancer *3*, 226–231.

Ly, J.D., Grubb, D.R., and Lawen, A. (2003). The mitochondrial membrane potential (deltapsi(m)) in apoptosis; an update. Apoptosis *8*, 115–128.

Mathelier, A., Fornes, O., Arenillas, D.J., and Chen, C. (2015). JASPAR 2016: a major expansion and update of the open-access database of transcription factor binding profiles. Nucleic Acids ….

Nagy, J.D., Victor, E.M., and Cropper, J.H. (2007). Why don“t all whales have cancer? A novel hypothesis resolving Peto”s paradox. Integr. Comp. Biol. *47*, 317–328.

Nunney, L. (1999). Lineage selection and the evolution of multistage carcinogenesis. Proc. Biol. Sci. *266*, 493–498.

Pertea, M., Pertea, G.M., Antonescu, C.M., Chang, T.-C., Mendell, J.T., and Salzberg, S.L. (2015). StringTie enables improved reconstruction of a transcriptome from RNA-seq reads. Nat. Biotechnol. *33*, 290–295.

Peto, R. (2015). Quantitative implications of the approximate irrelevance of mammalian body size and lifespan to lifelong cancer risk. Philos. Trans. R. Soc. Lond., B, Biol. Sci. *370*.

R Peto, F.J.R.P.N.L.L.L.J.C. (1975). Cancer and ageing in mice and men. British Journal of Cancer *32*, 411.

Rathjen, P.D., Toth, S., Willis, A., Heath, J.K., and Smith, A.G. (1990). Differentiation inhibiting activity is produced in matrix-associated and diffusible forms that are generated by alternate promoter usage. Cell *62*, 1105–1114.

Reddy, P.C., Sinha, I., Kelkar, A., Habib, F., Pradhan, S.J., Sukumar, R., and Galande, S. (2015). Comparative sequence analyses of genome and transcriptome reveal novel transcripts and variants in the Asian elephant Elephas maximus. J. Biosci. *40*, 891–907.

Rohland, N., Reich, D., Mallick, S., Meyer, M., Green, R.E., Georgiadis, N.J., Roca, A.L., and Hofreiter, M. (2010). Genomic DNA sequences from mastodon and woolly mammoth reveal deep speciation of forest and savanna elephants. PLoS Biol. *8*, e1000564.

Sela, I., Ashkenazy, H., Katoh, K., and Pupko, T. (2015). GUIDANCE2: accurate detection of unreliable alignment regions accounting for the uncertainty of multiple parameters. Nucleic Acids Res. *43*, W7–W14.

Sulak, M., Fong, L., Mika, K., Chigurupati, S., Yon, L., Mongan, N.P., Emes, R.D., and Lynch, V.J. (2016). TP53 copy number expansion is associated with the evolution of increased body size and an enhanced DNA damage response in elephants. eLife *5*.

Tait, S.W.G., and Green, D.R. (2010). Mitochondria and cell death: outer membrane permeabilization and beyond. Nat. Rev. Mol. Cell Biol. *11*, 621–632.

Vaseva, A.V., Marchenko, N.D., Ji, K., Tsirka, S.E., Holzmann, S., and Moll, U.M. (2012). p53 opens the mitochondrial permeability transition pore to trigger necrosis. Cell *149*, 1536–1548.

Voyle, R.B., Haines, B.P., Pera, M.F., Forrest, R., and Rathjen, P.D. (1999). Human germ cell tumor cell lines express novel leukemia inhibitory factor transcripts encoding differentially localized proteins. Exp. Cell Res. *249*, 199–211.

Wertheim, J.O., Murrell, B., Smith, M.D., Kosakovsky Pond, S.L., and Scheffler, K. (2015). RELAX: Detecting Relaxed Selection in a Phylogenetic Framework. Mol. Biol. Evol. *32*, 820–832.

Yona, A.H., Alm, E.J., and Gore, J. (2017). Random Sequences Rapidly Evolve Into De Novo Promoters. bioRxiv.

Table 1 RELAX(ed selection test) summary for duplicate LIF genes. Test for selection relaxation (K = 0.35) was significant (P=6.35×10^{-12}, LR = 47.22). log L, log likelihood of the model. # par., number of model parameters. AICc, Aikakie Information Criterion. Ltree, tree length. Branch set: LIF, canonical LIF genes; Pseudogene, LIF pseudogenes other than Proboscidean LIF6 genes. ω, d_N/d_S rate (percentage of sites in each site class).

Model	log L	# par.	AICc	Ltree	Branch set	ω1	ω2	ω3
Partitioned MG94xREV	-6201.45	92	12590.28	4.65	LIF	0.197 (100%)		
					Pseudogene	0.647 (100%)		
General Descriptive	-6117.12	170	12585.92	73.36	All	0.000114 (61%)	0.882 (37%)	9980 (1.2%)
Null	-6184.91	95	12563.43	88.03	LIF	0.248 (64%)	0.925 (36%)	1090 (0.43%)
					Pseudogene	0.248 (64%)	0.925 (36%)	1090 (0.43%)
Alternative	-6161.3	96	12518.29	36.98	LIF	0.00862 (17%)	0.233 (83%)	10000 (0.49%)
					Pseudogene	0.189 (17%)	0.600 (83%)	25.3 (0.49%)
Partitioned Exploratory	-6153.96	100	12511.92	26.63	LIF	0.000100 (63%)	0.485 (37%)	1470 (0.20%)
					Pseudogene	0.236 (47%)	0.934 (52%)	25.3 (1.0%)

Table 2 RELAX(ed selection test) summary for Proboscidean LIF6 genes. Test for selection intensification (K = 50.00) was significant (P=0.0347, LR = 4.46). log L, log likelihood of the model. # par., number of model parameters. AICc, Aikakie Information Criterion. Ltree, tree length. Branch set: LIF, non-Proboscidean LIF genes; LIF6, Proboscidean LIF6 genes. ω, d_N/d_S rate (percentage of sites in each site class).

Model	log L	# par.	AICc	Ltree	Branch set	ω1	ω2	ω3
Partitioned MG94xREV	-6201.45	92	12590.28	4.65	LIF	0.197 (100%)		
					LIF6	0.647 (100%)		
General Descriptive	-6117.12	170	12585.92	73.36	All	0.000114 (61%)	0.882 (37%)	9980 (1.2%)
Null	-6184.91	95	12563.43	88.03	LIF	0.248 (64%)	0.925 (36%)	1090 (0.43%)
					LIF6	0.248 (64%)	0.925 (36%)	1090 (0.43%)
Alternative	-6161.3	96	12518.29	36.98	LIF	0.00862 (17%)	0.233 (83%)	10000 (0.49%)
					LIF6	0.189 (17%)	0.600 (83%)	25.3 (0.49%)
Partitioned Exploratory	-6153.96	100	12511.92	26.63	LIF	0.000100 (63%)	0.485 (37%)	1470 (0.20%)
					LIF6	0.236 (47%)	0.934 (52%)	25.3 (1.0%)

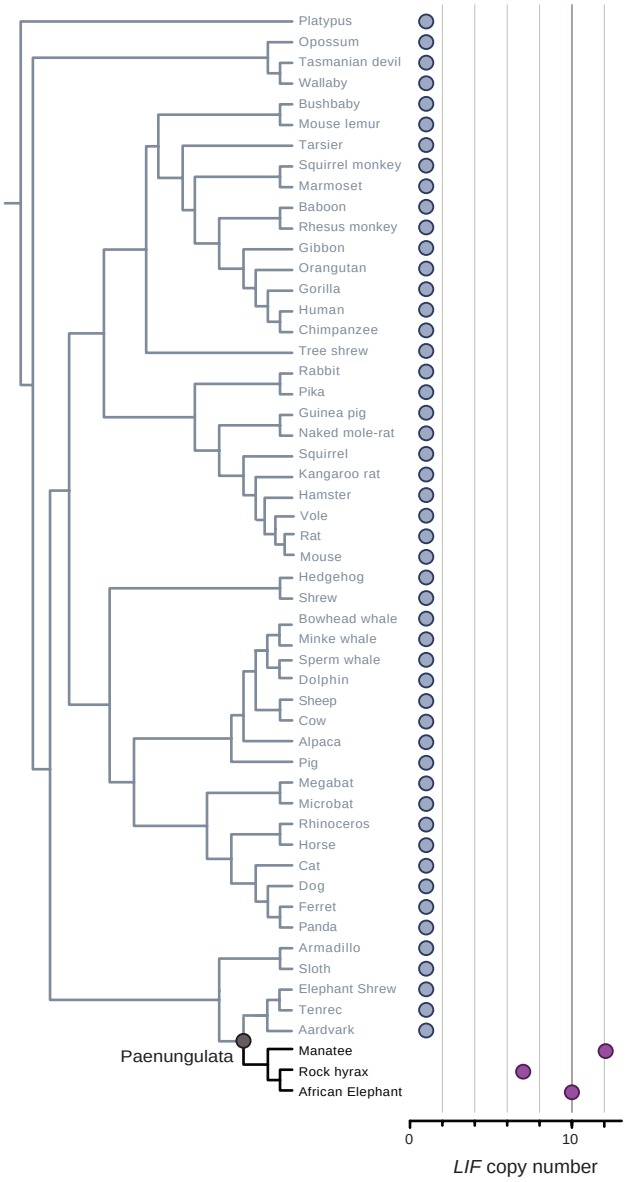

Figure 1. Expansion of *LIF* copy number in Paenungulata. *LIF* copy number in mammalian genomes. Clade names are shown for lineages in which the genome encodes more than one *LIF* gene or pseudogene.

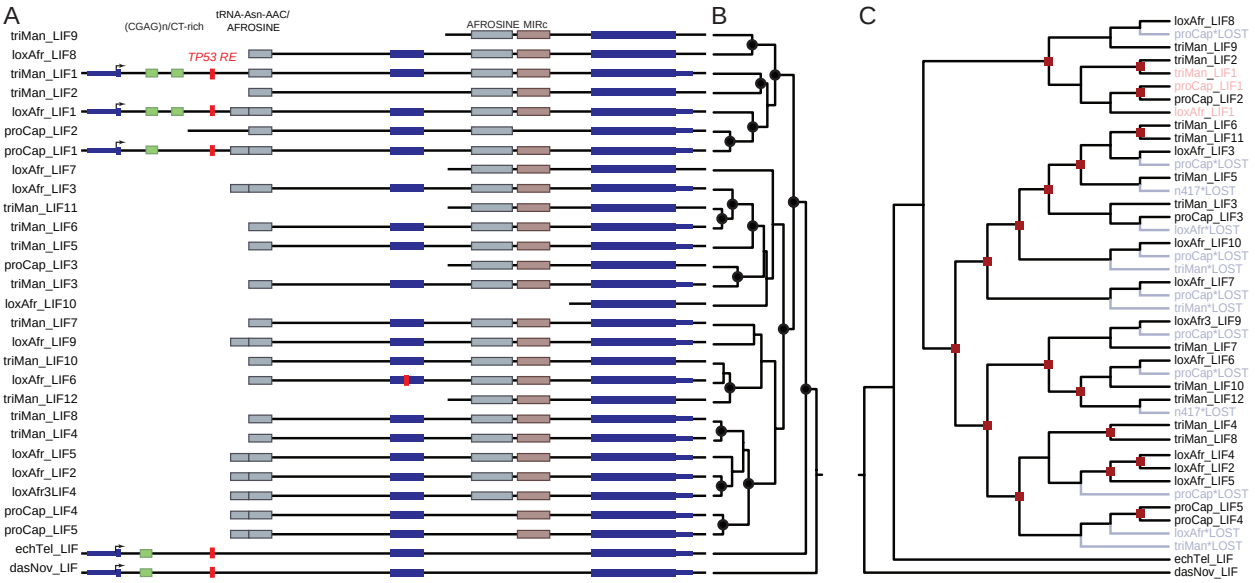

Figure 2. *LIF* copy number increased through segmental duplications.

(A) Organization of the *LIF* loci in African elephant (loxAfr), hyrax (ProCap), and manatee (triMan), tenrec (echTel), and armadillo (dasNov) genomes. The location of homologous transposable elements around *LIF* genes and TP53 transcription factor binding sites are shown.

(B) *LIF* gene tree, nodes with Bayesian Posterior Probabilities (BPP) > 0.9 are indicated with black circles.

(C) Reconciled *LIF* gene trees African elephant (loxAfr), hyrax (ProCap), and manatee (triMan). Duplication events are indicated with red squares, gene loss events are indicated with in blue and noted with '*LOST'. Cannonical *LIF* genes (*LIF1*) are shown in red.

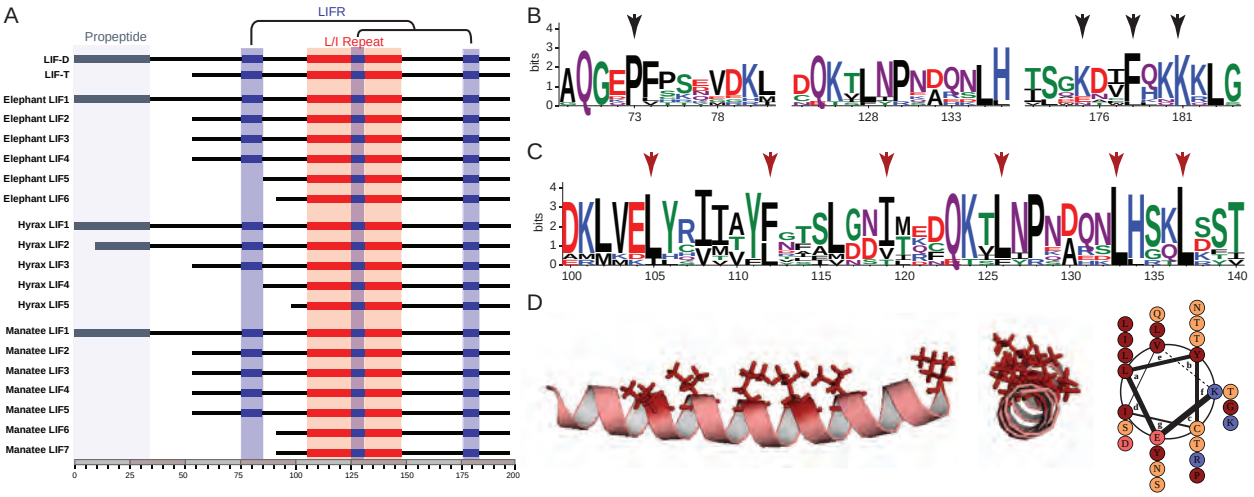

Figure 3. Structure of duplicate LIF genes with coding potential.

(A) Domain structure the LIF-D and LIF-T isoforms and of duplicate elephant, hyrax, and manatee LIF duplicates with coding potential. Locations of the propeptide, interactions sites with the LIF receptor (LIFR), and L/I repeat are shown.

(B) Conservation of LIF receptor (LIFR) interaction sites in duplicate LIF proteins. Residues in LIF that make physical contacts with LIFR are indicated with black arrows.

(C) Conservation of the leucine/isoleucine repeat region in duplicate LIF proteins. Leucine/isoleucine residues required for pro-apoptotic functions of LIF-T are indicated with red arrows.

(D) Leucine/isoleucine residues in the African elephant LIF6 form an amphipathic alpha helix. Structural model of the LIF6 protein (left, center), and helical wheel representation of the LIF6 amphipathic alpha helix.

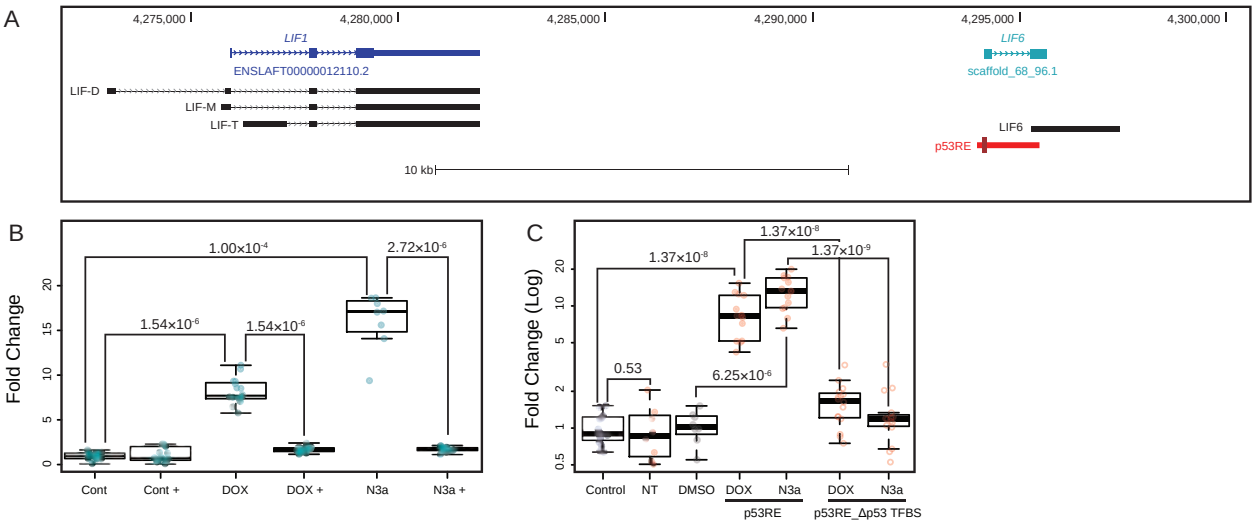

Figure 4. African elephant LIF6 is transcriptionally up-regualted by p53 in response to DNA damage.

(A) Structure of the African elephant *LIF*/*LIF6* locus (loxAfr3). The ENSEMBL LIF and geneID gene models are shown in blue and cyan. Transcripts assembled by StringTie (option 'do not use GFF/GTF') are shown in black. The region upstream of LIF6 used in transcription factor binding site prediction and luciferase assays is shown in red; the location of the putative p53 binding site is shown in dark red.

(B) Quantitative real-time PCR showing that *LIF6* is up-regulated in African elephant fibroblasts in response to doxorubicin (DOX) or nutlin-3a treatment (N3a), siRNA mediated p53 knockdown prevents *LIF6* up-regulation in response to doxorubicin (DOX+) or nutlin-3a treatment (N3a+). N=16, Wilcox test.

(C) Dual luciferase reporter assay indicates that the LIF6 upstream region activates luciferase expression in African elephant fibroblasts in response to doxorubicin (DOX) or nutlin-3a treatment (N3a), and is significantly attenuated by deletion of the putative p53 binding site (p53RE_Δp53 TFBS). DMSO, carrier for nutlin-3a. N=14-16, Wilcox test.

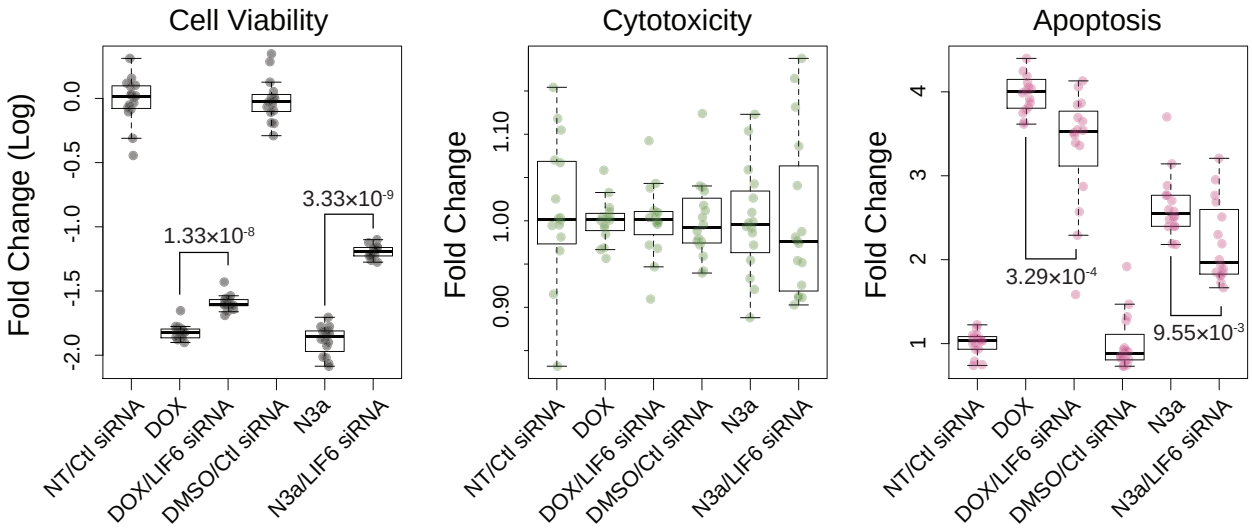

Figure 5. African elephant LIF6 contributes to the augmented DNA damage response in elephants. African elephant fibroblasts were treated with either doxorubicin (DOX) or nutlin-3a (N3a), or 3 siRNAs targeting LIF6 and doxorubicin (DOX/LIF6 siRNA) or nutlin-3a treatment (N3a/LIF6 siRNA). Cell viability, cytoxicity, and the induction of apoptosis was assayed using an ApoTox-Glo assay 24 hours after treatment. NT, no treatment. Ctl siRNA, negative control siRNA. DMSO, carrier for nutlin-3a. N=16, Wilcox test.

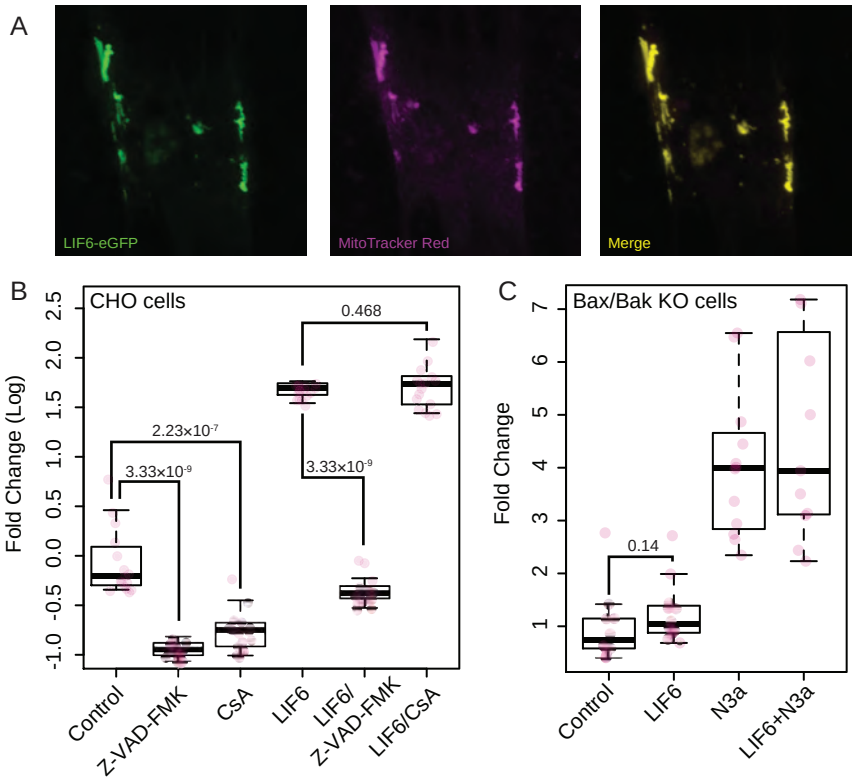

Figure 6. African elephant LIF6 is mitochondrial localized and induces caspase dependent apoptosis.

(A) African elephant fibroblasts were transiently transfected with an expression vector encoding a eGFP tagged *LIF6* gene and mitochondria stained with MitoTracker Red CM-H2XRos. A single representative cell is shown.

(B) Chinese hamster ovary (CHO) cells (which do not express LIFR) were transiently transfected with an expression vector encoding the African elephant *LIF6* gene and assayed for the induction of apoptosis with an ApoTox-Glo assay 24 hours after transfection. Induction of apoptosis by LIF6 was inhibited by co-treatment with the irreversible broad-spectrum caspase inhibitor Z-VAD-FMK but not cyclosporine-A (CsA). Treatment of CHO cells with Z-VAD-FMK or CsA alone reduced apoptosis. N=16, Wilcox test.

(C) Over-expression of LIF6 in Bax/Bak double knockout mouse embryonic fibroblasts does not induce apoptosis, not augmented nutlin-3a induced apoptosis. N=8, Wilcox test.

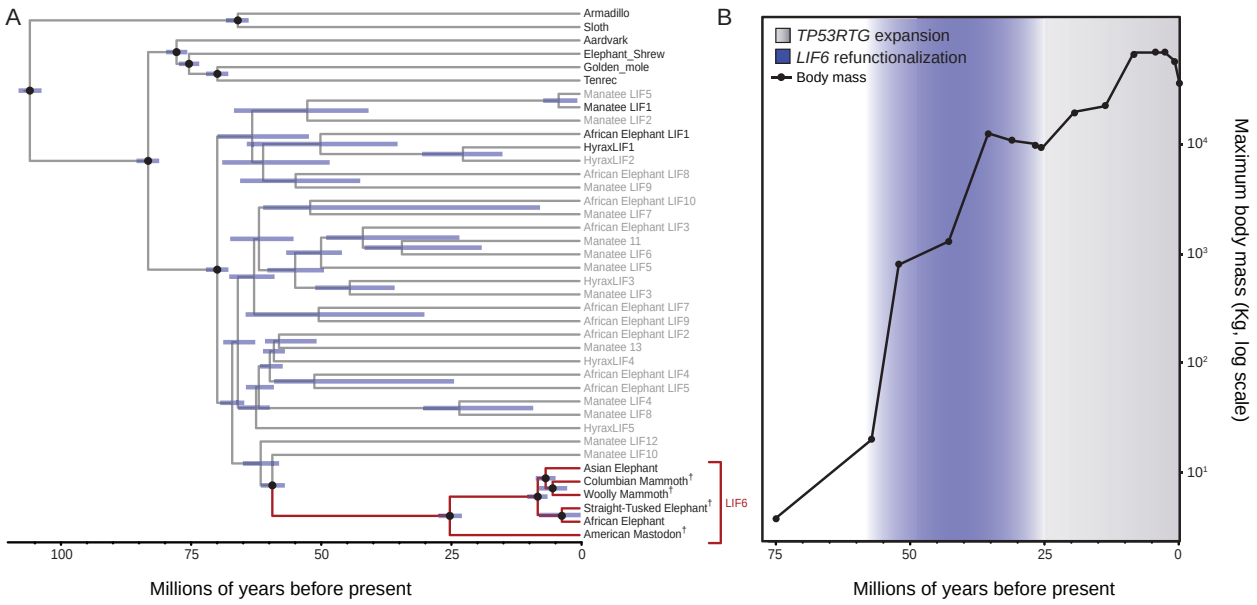

Figure 7. LIF6 is a re-functionalized pseudogene.

(A) Time calibrated Bayesian phylogeny of Atlantogenatan LIF genes. The Proboscidean LIF6 clade is highlighted in red, canonical LIF genes in black, LIF duplicates in grey. The 95% highest posterior density (HPD) of estimated divergence dates are shown as blue bars. Nodes used to calibrate divergence dates are shown with black circles.

(B) Proboscidean LIF6 re-functionalized during the evolution of large body sizes in the Proboscidean lineage.